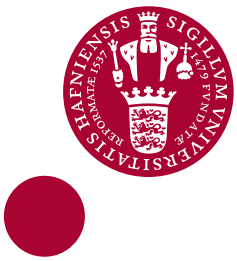

ER Stress Inhibits Liver Fatty Acid Oxidation while Unmitigated Stress Leads to Anorexia-Induced Lipolysis and Both Liver and Kidney Steatosis

DeZwaan-McCabe, Diane; Sheldon, Ryan D; Gorecki, Michelle C; Guo, Deng-Fu; Gansemer, Erica R; Kaufman, Randal J; Rahmouni, Kamal; Gillum, Matthew P; Taylor, Eric B; Teesch, Lynn M; Rutkowski, D Thomas

Published in:
Cell Reports

DOI:
10.1016/j.celrep.2017.05.020

Publication date:
2017

Document version
Publisher's PDF, also known as Version of record

Article

Cell Reports

ER Stress Inhibits Liver Fatty Acid Oxidation while Unmitigated Stress Leads to Anorexia-Induced Lipolysis and Both Liver and Kidney Steatosis

Graphical Abstract

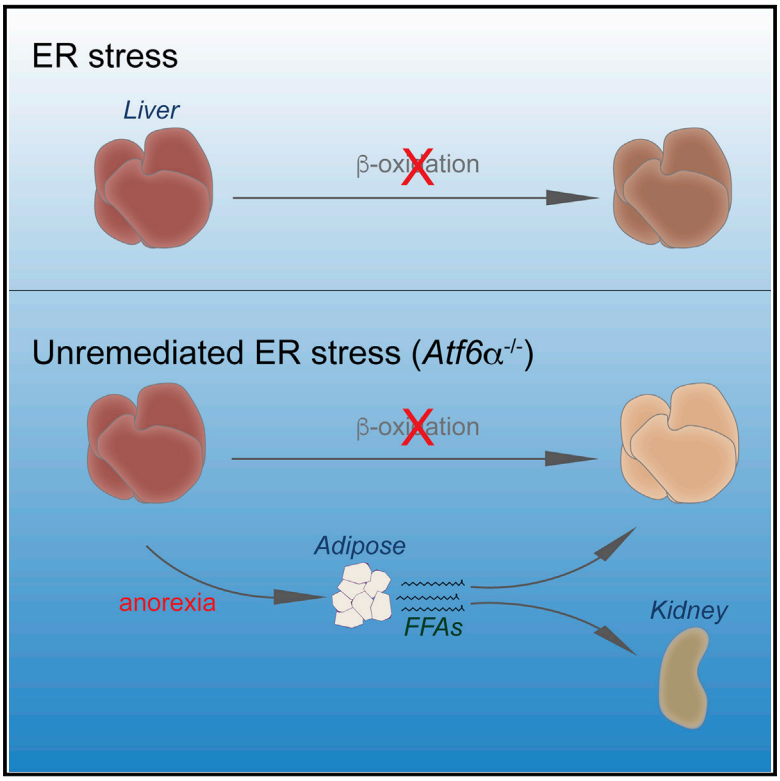

Authors

Diane DeZwaan-McCabe, Ryan D. Sheldon, Michelle C. Gorecki, ..., Eric B. Taylor, Lynn M. Teesch, D. Thomas Rutkowski

Correspondence

thomas-rutkowski@uiowa.edu

In Brief

The mechanisms by which the liver and kidney become steatotic when challenged by ER stress are not known. DeZwaan-McCabe et al. show that ER stress inhibits fatty acid oxidation in the liver and that unmitigated stress causes anorexia and promotes adipose lipolysis and further steatosis in the liver and kidney.

Highlights

- ER stress directly targets the liver and kidneys, and both organs accumulate lipid
- Inhibition of fatty acid oxidation contributes to hepatic steatosis
- Animals that cannot mitigate ER stress become anorexic
- Lipolysis exacerbates steatosis in the liver and kidney of sensitive animals

DeZwaan-McCabe et al., 2017, Cell Reports *19*, 1794–1806
May 30, 2017
http://dx.doi.org/10.1016/j.celrep.2017.05.020

OPEN ACCESS
CellPress

Cell Reports
Article

ER Stress Inhibits Liver Fatty Acid Oxidation while Unmitigated Stress Leads to Anorexia-Induced Lipolysis and Both Liver and Kidney Steatosis

Diane DeZwaan-McCabe,[1,2,9] Ryan D. Sheldon,[2,3] Michelle C. Gorecki,[4] Deng-Fu Guo,[2,5] Erica R. Gansemer,[1,2] Randal J. Kaufman,[6] Kamal Rahmouni,[2,5,7] Matthew P. Gillum,[4] Eric B. Taylor,[2,3] Lynn M. Teesch,[8] and D. Thomas Rutkowski[1,2,7,10,*]

[1]Department of Anatomy and Cell Biology
[2]Fraternal Order of Eagles Diabetes Research Center
[3]Department of Biochemistry
Carver College of Medicine, University of Iowa, Iowa City, IA 52242, USA
[4]Section for Metabolic Imaging and Liver Metabolism, the Novo Nordisk Foundation Center for Basic Metabolic Research, University of Copenhagen, 2200 Copenhagen N, Denmark
[5]Department of Pharmacology, Carver College of Medicine, University of Iowa, Iowa City, IA 52242, USA
[6]Degenerative Diseases Program, SBP Medical Discovery Institute, La Jolla, CA 92037, USA
[7]Department of Internal Medicine, Carver College of Medicine, University of Iowa, Iowa City, IA 52242, USA
[8]High Resolution Mass Spectrometry Facility, University of Iowa, Iowa City, IA 52242, USA
[9]Present address: Exemplar Genetics, Coralville, IA 52241, USA
[10]Lead Contact
*Correspondence: thomas-rutkowski@uiowa.edu
http://dx.doi.org/10.1016/j.celrep.2017.05.020

SUMMARY

The unfolded protein response (UPR), induced by endoplasmic reticulum (ER) stress, regulates the expression of factors that restore protein folding homeostasis. However, in the liver and kidney, ER stress also leads to lipid accumulation, accompanied at least in the liver by transcriptional suppression of metabolic genes. The mechanisms of this accumulation, including which pathways contribute to the phenotype in each organ, are unclear. We combined gene expression profiling, biochemical assays, and untargeted lipidomics to understand the basis of stress-dependent lipid accumulation, taking advantage of enhanced hepatic and renal steatosis in mice lacking the ER stress sensor ATF6α. We found that impaired fatty acid oxidation contributed to the early development of steatosis in the liver but not the kidney, while anorexia-induced lipolysis promoted late triglyceride and free fatty acid accumulation in both organs. These findings provide evidence for both direct and indirect regulation of peripheral metabolism by ER stress.

INTRODUCTION

Endoplasmic reticulum (ER) stress is caused by an imbalance between the need to properly fold newly synthesized secretory and membrane proteins and the capacity of the organelle to do so. Accordingly, unfolded protein response (UPR) activation alleviates ER stress by both transcriptional and non-transcriptional mechanisms that, together, diminish protein load and enhance the ability of the organelle to properly fold, transport, or degrade client proteins (Walter and Ron, 2011; Wang and Kaufman, 2016). As ER protein folding is a fundamental cellular process, the upregulation of genes encoding ER chaperones, trafficking factors, and ER-associated degradation (ERAD) components is conserved from one cell type to another and from yeast to humans (Arensdorf et al., 2013b).

In the liver, ER stress leads to lipid accumulation, or hepatic steatosis (Rutkowski et al., 2008; Yamamoto et al., 2010; Zhang et al., 2011), indicating that ER stress and/or UPR activation regulates, directly or indirectly, lipid metabolism in that organ. This steatosis can be elicited by overexpression of a difficult-to-fold protein (Rutkowski et al., 2008); proteasome inhibition (Chikka et al., 2013); or, most robustly, inhibition of the ER-specific post-translational modification N-linked glycosylation using the drug tunicamycin (TM) (Lee et al., 2012; Rutkowski et al., 2008). Necessarily, ER stress must elicit hepatic steatosis by decreased lipid efflux or catabolism, by increased synthesis or uptake, or by some combination of these. ER stress is known to impair the secretion of very low-density lipoprotein (VLDL) from the liver (Ota et al., 2008; Rutkowski et al., 2008; Wang et al., 2012; Yamamoto et al., 2010). VLDL particles are assembled in the ER by the coalescence of triglyceride and cholesterol around the ER client protein apolipoprotein B100 (Gibbons et al., 2004). Failure to secrete triglycerides in the form of VLDL particles doubtless contributes to stress-induced hepatic steatosis.

ER stress in the liver also leads to substantial and coordinated regulation of genes involved in lipid metabolism, including both anabolism and catabolism (Arensdorf et al., 2013a; Rutkowski et al., 2008). However, the contributions of lipogenesis and fatty

acid oxidation (FAox) in vivo are not known, since the actual activity of these pathways has not been assessed. Importantly, ER stress has been implicated in a number of chronic diseases that result in lipid dysregulation, including obesity (Özcan et al., 2004), alcoholism (Ji, 2014), viral hepatitis (Chan, 2014), and others. Thus, the mechanisms leading from ER stress to lipid dysregulation are of considerable physiological importance.

ER stress is sensed by three pathways, and two of these—mediated by PERK (PKR-like ER kinase) and IRE1α (Inositol-requiring enzyme 1α)—are essential in vertebrates (Harding et al., 2001; Zhang et al., 2011). However, animals lacking the third sensor, ATF6α (Activating transcription factor 6α), are viable and overtly normal (Gomez et al., 2014). ATF6α augments the transcriptional upregulation of ER chaperones and ERAD factors but is not strictly essential for the upregulation of most of these (Adachi et al., 2008; Wu et al., 2007; Yamamoto et al., 2007). Accordingly, cells lacking ATF6α are capable of initially responding appropriately to ER stress but become progressively impaired as ER stress persists, due to their inability to resolve the stress (Wu et al., 2007). As a consequence, animals lacking ATF6α, while having no apparent basal phenotype, are sensitive to a number of experimental ER stressors (Azuma et al., 2014; Cao et al., 2013; Egawa et al., 2011; Usui et al., 2012; Wu et al., 2011; Yoshikawa et al., 2015). This sensitivity includes challenge with TM, which, in *Atf6*$\alpha^{-/-}$ animals, leads to not only profoundly fatty liver but also to fat accumulation in the kidney (renal steatosis)—which occurs much less prominently, if at all, in wild-type animals—and eventually, within 72–96 hr, to death (Wu et al., 2007). We used the *Atf6*$\alpha^{-/-}$ animals, hypersensitive to stress, as a tool to identify the pathways by which ER stress leads to lipid accumulation in these two distinct organs.

RESULTS

ER Stress Induces Lipid Accumulation in Liver and Kidneys of *Atf6*$\alpha^{-/-}$ Mice

To better characterize ER stress-induced hepatic and renal steatosis, we treated wild-type and *Atf6*$\alpha^{-/-}$ mice with the ER stressor TM. While other stressors, such as hepatic overexpression of a difficult-to-fold protein or proteasome inhibition, also lead to steatosis and similar changes in the expression of metabolic genes as TM (Chikka et al., 2013; Rutkowski et al., 2008), TM is the most robust and specific ER stressor in vivo. TM robustly targets the liver and kidneys, as shown by splicing of the target of the IRE1 endonuclease, *Xbp1* mRNA (Figure 1A).

In our previous work, we showed that TM treatment leads to hepatic lipid accumulation as rapidly as 8 hr after challenge (Arensdorf et al., 2013a). Here as well, TM led to hepatic triglyceride accumulation in both wild-type and *Atf6*$\alpha^{-/-}$ animals, and this accumulation became even more pronounced specifically in *Atf6*$\alpha^{-/-}$ animals at later times after challenge. This accumulation was seen in both direct measurement of hepatic triglyceride (Figure 1B) and immunostaining for the lipid droplet marker protein ADRP (Figure 1C). Thus, hepatic steatosis initially occurs in both wild-type and *Atf6*$\alpha^{-/-}$ animals but is exacerbated at later times in the knockouts.

In contrast to the liver, TM-induced renal lipid accumulation was restricted to *Atf6*$\alpha^{-/-}$ animals. Oil red O staining, which detects neutral lipids, revealed very little accumulation in wild-type animals but it did reveal substantial steatosis in the tubule cells in *Atf6*$\alpha^{-/-}$ animals, particularly 48 hr after challenge (Figure 1D). These findings were mirrored by ADRP immunostaining of the kidneys (Figure 1E).

Lipogenesis Does Not Contribute to Early Hepatic Steatosis

Previous reports in cultured hepatocytes and other cell types have suggested that ER stress stimulates lipogenesis (Colgan et al., 2007; Lee et al., 2012). However, our own work has suggested that important genes of the lipogenic pathway are downregulated by ER stress (Arensdorf et al., 2013a), consistent with other studies suggesting an anti-lipogenic effect of ER stress (Herrema et al., 2016; Wang et al., 2012). Despite this finding, it is possible that stress stimulates lipogenesis only during a transient window that has been previously overlooked. Thus, we first examined in wild-type and *Atf6*$\alpha^{-/-}$ animals the expression of genes encoding both transcriptional master regulators of lipogenesis and cholesterologenesis (*Srebf1*, *Srebf2*, respectively) and the important and rate-limiting enzymes in both processes (*Acaca*, *Fasn*, *Scd1*, and *Hmgcr*). The lipogenic genes (*Srebf1*, *Acaca*, *Fasn*, and *Scd1*) were robustly suppressed by ER stress to comparable extents in both wild-type and *Atf6*$\alpha^{-/-}$ animals at all time points examined (Figure 2A). The cholesterologenic genes (*Srebf2* and *Hmgcr*) were somewhat discrepant between the two genotypes but did not show any evidence of being upregulated (Figure 2A).

We next directly assessed lipogenic activity at early and later points after ER stress induction, monitoring the conversion of ^{14}C-acetate into ^{14}C-fatty acid by liver homogenates. We monitored metabolic activity at both early time points (8 hr) in wild-type animals and at later points in both wild-type and *Atf6*$\alpha^{-/-}$ animals, when the latter specifically begin to show both exacerbated liver ER stress and enhanced hepatic steatosis (e.g., Figure 1B; (Arensdorf et al., 2013a). As a positive control, we first confirmed that treating animals with insulin yielded the expected increase in lipogenic activity (Jones, 2016) (Figure 2B). However, no significant increase in lipogenic activity was seen in wild-type mice (Figure 2C) or *Atf6*$\alpha^{-/-}$ mice (data not shown) 8 hr after challenge or in wild-type mice 24 hr after challenge (Figure 2D). We did, however, detect an increase in lipogenic activity in *Atf6*$\alpha^{-/-}$ animals 24 hr after challenge (Figure 2E). Given the substantial suppression of lipogenic genes in these animals (Figure 2A), this finding was unexpected and awaits further studies to explain. In any case, these results suggest that lipogenesis is not a meaningful early contributor to ER stress-induced hepatic steatosis in wild-type mice, although it might contribute at a later phase.

ER Stress Suppresses Hepatic FAox

We next used a similar genetic and biochemical approach to ask whether FAox contributes to hepatic steatosis. We found that the transcriptional master regulator of FAox, Peroxisome Proliferator Activated Receptor Alpha (*Ppara*), was suppressed ~2-fold by ER stress in wild-type animals, while it was suppressed ~8-fold in *Atf6*$\alpha^{-/-}$ animals (Figure 3A). Genes encoding key steps in beta-oxidation (*Cpt1a*, *Acadm*), peroxisomal

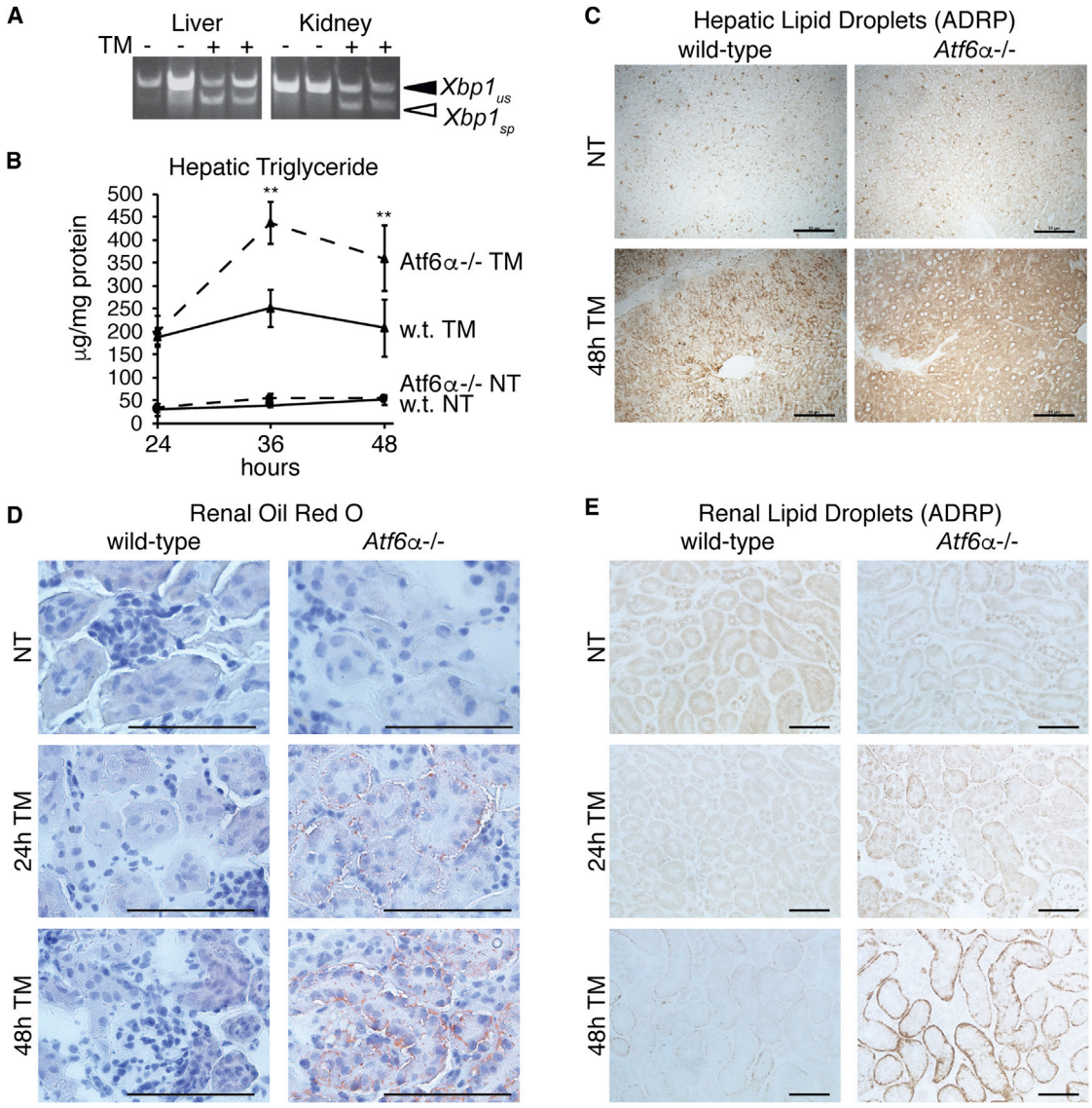

Figure 1. TM Treatment Causes Hepatic and Renal Steatosis in Atf6α$^{-/-}$ Mice

(A) Mice were challenged with vehicle or 1 mg/kg TM as indicated for 8 hr, and RNA was prepared from liver and kidneys. *Xbp1* mRNA splicing was detected by conventional RT-PCR, with spliced (sp) and unspliced (us) forms indicated.

(B) Wild-type or *Atf6α*$^{-/-}$ mice were challenged with vehicle or 1 mg/kg TM, and triglyceride levels were measured in liver lysates at the indicated times following injection. Significances compare *Atf6α*$^{-/-}$ and wild-type (w.t.) TM-treated animals. n = 3–4 animals per group. Throughout the article, graphs present data as means ± SD. **p < 0.01.

(C) Formalin-fixed liver sections from wild-type or *Atf6α*$^{-/-}$ animals treated with TM for 48 hr were stained for the lipid droplet marker protein ADRP. Representative images are shown. Scale bars, 50 μm.

(D) Fresh frozen kidney sections from wild-type or *Atf6α*$^{-/-}$ animals treated for 24 or 48 hr with TM were stained with the neutral lipid stain oil red O. Representative images are shown. Scale bars, 50 μm.

(E) Formalin-fixed kidney sections from animals treated as in (D) were stained for the lipid droplet marker protein ADRP as in (C). Representative images are shown. Scale bars, 50 μm.

NT, not treated.

oxidation (*Acox1*), and microsomal oxidation (*Cyp4a10*) were not suppressed in wild-type animals but were significantly suppressed in *Atf6α*$^{-/-}$ animals (Figure 3A).

To directly assess FAox activity, we monitored the conversion of ^{14}C-palmitate into $^{14}CO_2$; as expected, this conversion was significantly reduced by the CPT1 inhibitor etomoxir (ET) (Figure 3B). Using this assay to monitor FAox activity in liver homogenates, we found that FAox was suppressed by approximately 50% in wild-type animals 8 hr after challenge (Figure 3C). Supporting this finding, serum levels of the ketone

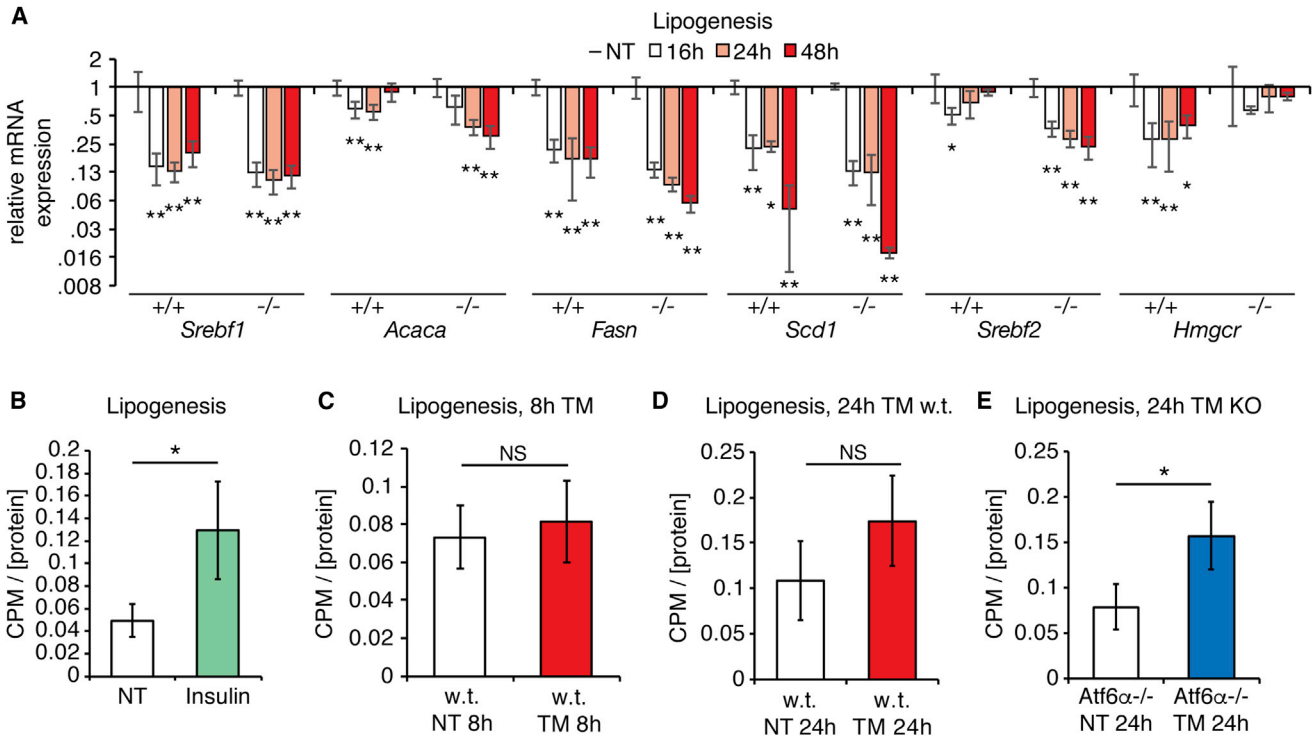

Figure 2. TM Suppresses Lipogenic Genes and Does Not Affect Hepatic Lipogenic Activity at Early Times after Challenge

(A) The expression of the indicated lipogenic and cholesterologenic genes was measured by qRT-PCR from the livers of wild-type or *Atf6α*$^{-/-}$ animals challenged with TM for the indicated times. Significances were determined relative to unchallenged animals of the same genotype. n = 3.

(B) Wild-type mice were treated with 2 U human insulin for 1 hr, and lipogenic activity relative to homogenate protein concentration was measured in liver homogenates by conversion of ^{14}C-acetate into ^{14}C-fatty acid as described in Experimental Procedures. n = 3.

(C) Wild-type (w.t.) mice were treated with TM for 8 hr, and hepatic lipogenic activity was measured as in (B). n = 3.

(D) Wild-type mice were treated with TM for 24 hr, and then lipogenic activity was assessed as described earlier. n = 3.

(E) Same as in (D), except using *Atf6α*$^{-/-}$ animals. n = 3.

*p < 0.05; **p < 0.01; NS, not significant; NT, not treated; CPM, counts per minute.

body β-hydroxybutyrate, which is a by-product of hepatic FAox (Rui, 2014), were also diminished (Figure 3D). By 48 hr after challenge, FAox activity returned to normal levels in wild-type mice but remained suppressed in *Atf6α*$^{-/-}$ animals (Figure 3E).

Lipid accumulation due to impaired FAox could be due to dysregulation of β-oxidation in the mitochondria, to the inhibition of peroxisomal oxidation—which principally shortens very long chain fatty acids for entry into β-oxidation—or to both. We observed a significant decrease in the ability of isolated mitochondria from TM-treated *Atf6α*$^{-/-}$ animals to completely oxidize palmitate to CO_2 (Figure 3F). Instead, mitochondria from TM-treated animals accumulated acid-soluble metabolites, which are incompletely oxidized products of β-oxidation (Hirschey et al., 2011) (Figure 3G). The accumulation of these products suggests that TM impairs FAox at a point downstream of lipid shuttling into mitochondria and upstream of entry of acetyl-CoA (coenzyme A) into the tricarboxylic acid (TCA) cycle. Mitochondrial content did not differ between groups, as assessed by oxidative phosphorylation (OXPHOS) immunoblot (data not shown). We also observed that peroxisomal content was dramatically reduced in *Atf6α*$^{-/-}$, but not wild-type, animals 24 hr after challenge (Figure 3H). This finding was consistent with the profound genetic suppression of *Pparα*, which, as its name denotes, stimulates peroxisome proliferation. Taken together, these results show that ER stress inhibits FAox activity, likely at both mitochondrial and peroxisomal levels, and that this inhibition contributes to the early development of hepatic steatosis in both wild-type and knockout animals and to the late aggravation of hepatic steatosis in *Atf6α*$^{-/-}$ animals.

Neither Suppressed Catabolism nor Enhanced Anabolism Accounts for Kidney Steatosis

Given that liver-autonomous processes—namely, inhibition of VLDL secretion (Ota et al., 2008; Rutkowski et al., 2008; Wang et al., 2012; Yamamoto et al., 2010) and of FAox (Figure 3)—contribute to stress-induced hepatic steatosis, we asked whether renal steatosis might, likewise, occur through direct regulation of metabolism by ER stress in the kidney. Supporting our findings in Figure 1, we found that mRNA expression of the lipid droplet marker *Adrp*—the transcription of which is known to increase when intracellular lipid levels rise (Targett-Adams et al., 2005)—was increased in *Atf6α*$^{-/-}$ mice, but not wild-type mice, and that this induction was much more dramatic 48 hr after challenge (Figure 4A). Thus, by at least this readout,

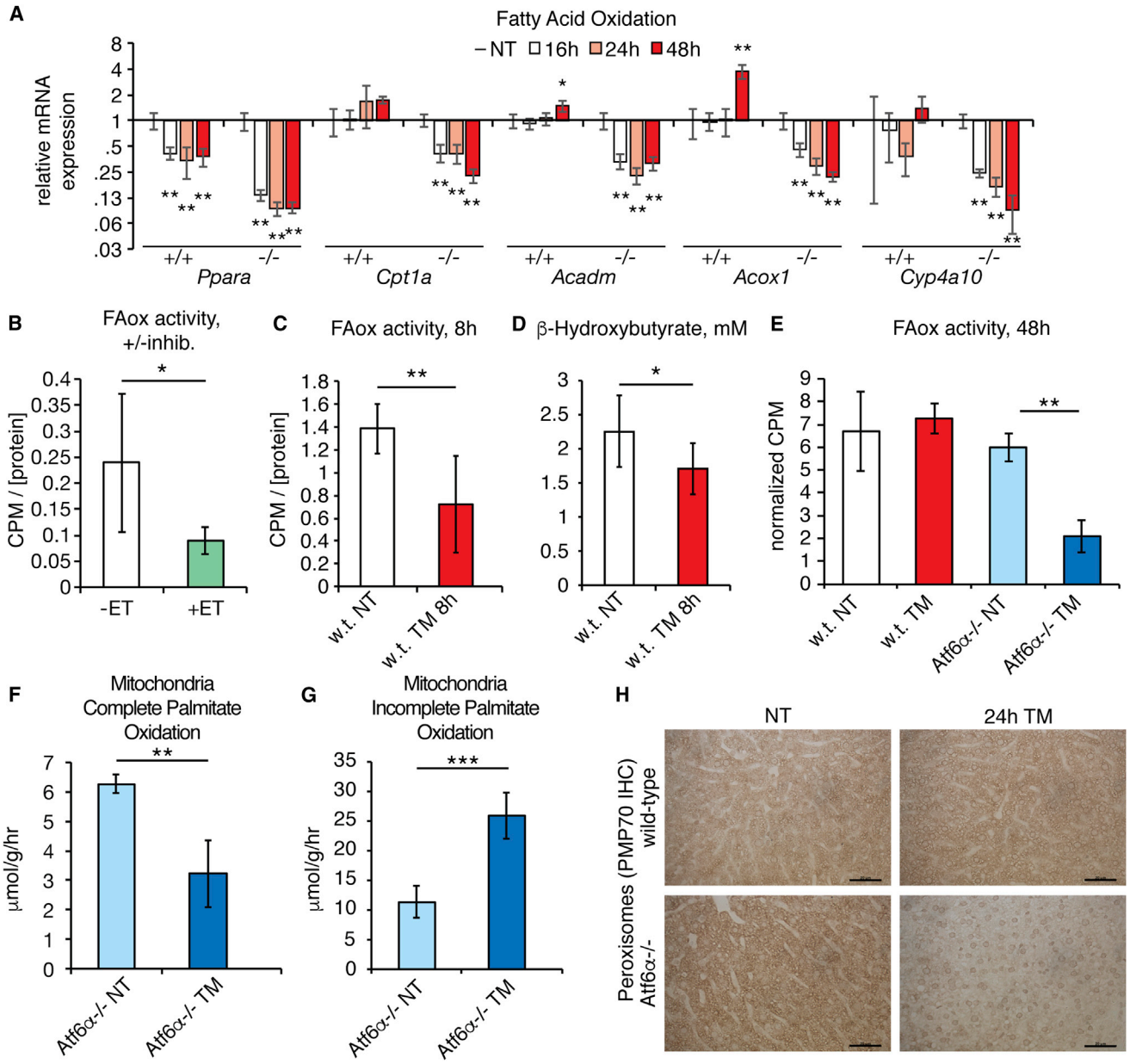

Figure 3. ER Stress Suppresses Hepatic FAox Activity

(A) Expression of the indicated FAox genes was assessed by qRT-PCR as in Figure 2A.

(B) Mice were fasted for 24 hr, and homogenates were isolated and divided into two aliquots, one of which was treated with the CPT1 inhibitor (inhib.) etomoxir (ET). FAox activity was measured as described in the Experimental Procedures. n = 6.

(C) Wild-type (w.t.) mice were fasted for 24 hr and treated with TM for the final 8 hr, and FAox activity was measured from liver homogenates as described earlier. n = 6–8.

(D) β-hydroxybutyrate levels were measured from the plasma of animals treated as in (C). n = 8–9.

(E) Wild-type or *Atf6*$\alpha^{-/-}$ animals were treated for 48 hr with TM, including fasting for the last 20 hr. Hepatic FAox activity was measured as described earlier. n = 3.

(F and G) *Atf6*$\alpha^{-/-}$ animals were treated for 48 hr with TM, and mitochondria were isolated from liver homogenates. Production of $^{14}CO_2$ (F) and acid-soluble metabolites (G) was measured as described in Experimental Procedures. n = 4.

(H) Peroxisome abundance was assessed by immunohistochemistry, using the marker PMP70, from animals treated for 24 hr with vehicle or 1 mg/kg TM. Representative data are shown. Scale bars, 20 μm.

*p < 0.05; **p < 0.01; ***p < 0.001; NT, not treated; CPM, counts per minute.

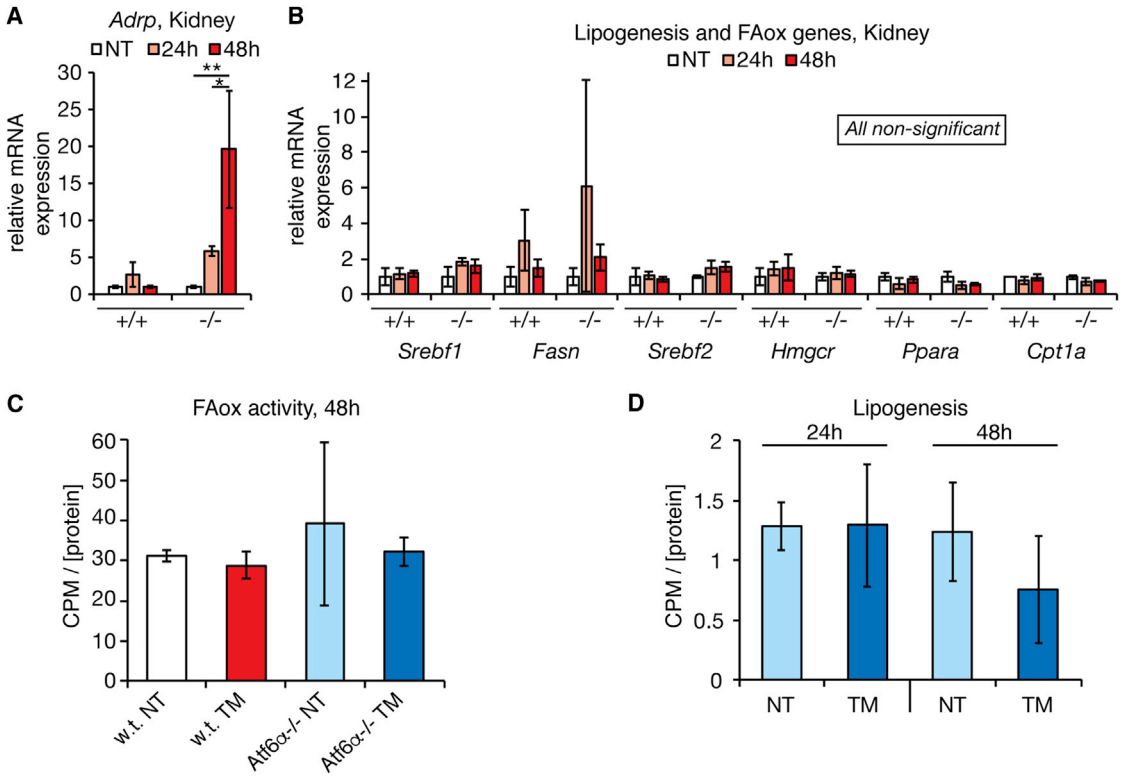

Figure 4. TM Treatment Does Not Alter Renal FAox or Lipogenic Activity

(A) qRT-PCR was used to assess the relative mRNA expression of the gene encoding the lipid droplet marker protein ADRP in kidneys of wild-type or *Atf6α*$^{-/-}$ animals treated for 24 or 48 hr with TM. *p < 0.05; **p < 0.01.

(B) Same as (A), except assessing expression of a representative sampling of metabolic genes regulating lipogenesis, cholesterologenesis, and FAox.

(C) FAox activity was measured as in Figure 3E, except using kidney homogenates. No significant differences were seen. n = 3. w.t., wild-type.

(D) Lipogenic activity was measured in *Atf6α*$^{-/-}$ animals as in Figure 2E. No significant differences were seen. n = 3.

NT, not treated; CPM, counts per minute.

there is transcriptional evidence of lipid dysregulation in the kidney. In contrast to the liver, however, a survey of genes involved in both lipogenesis and FAox revealed no significant changes in the kidney in either wild-type or knockout animals (Figure 4B; data not shown). Consistent with this finding, we observed no evidence that either FAox (Figure 4C) or lipogenesis (Figure 4D) was altered in the kidneys of *Atf6α*$^{-/-}$ mice, despite their extensive steatosis.

Lipid Mobilization from Adipose Likely Drives Late Hepatic and Renal Steatosis in *Atf6α*$^{-/-}$ Animals

Lacking direct evidence for altered lipid catabolism or anabolism in renal steatosis, we utilized an untargeted lipidomic approach with the goal of identifying potential pathways of lipid metabolism that might be dysregulated in *Atf6α*$^{-/-}$ animals and could underlie the steatosis phenotype. We also reasoned that this approach could identify lipid species other than the neutral lipids that are detected by oil red O staining and ADRP immunostaining, in the event that the effects of ER stress on lipid metabolism in these animals extend to other pathways. To do this, we challenged wild-type or knockout animals with TM for 48 hr, extracted lipids from kidney homogenates, and analyzed them by liquid chromatography-mass spectrometry (LC-MS) in both positive and negative modes (i.e., for the separation of anions or cations generated by electrospray ionization (ESI), with each mode preferentially detecting different classes of lipids). Resultant data were then processed using XCMS software to categorize and putatively identify altered lipid species.

Cloud plots of this analysis are shown in Figure 5, and putative lipid identifications are listed in Table 1. Consistent with the observation that wild-type animals accumulated very little renal fat upon TM treatment, these animals displayed comparable numbers of lipid species that were enhanced (Figure 5A, green circles) versus reduced (Figure 5, red circles) in the positive ion mode. In contrast, in response to TM treatment, *Atf6α*$^{-/-}$ animals displayed an enhanced abundance of a wide spectrum of lipid species, with particular enrichment for triglycerides and ceramides (Figure 5B; Table 1). The accumulation of triglycerides is consistent with enhanced lipid storage, but it shed little light on the source of those lipids, since lipid accumulation in this case was best explained by small accumulations of many diverse lipid species, rather than unique accumulation of one or a few such species. The accumulation of ceramides was accompanied by the upregulation of *Sptlc1*, which encodes the rate-limiting enzyme in ceramide synthesis, and also by enhanced TUNEL staining indicative of cell death, known to be

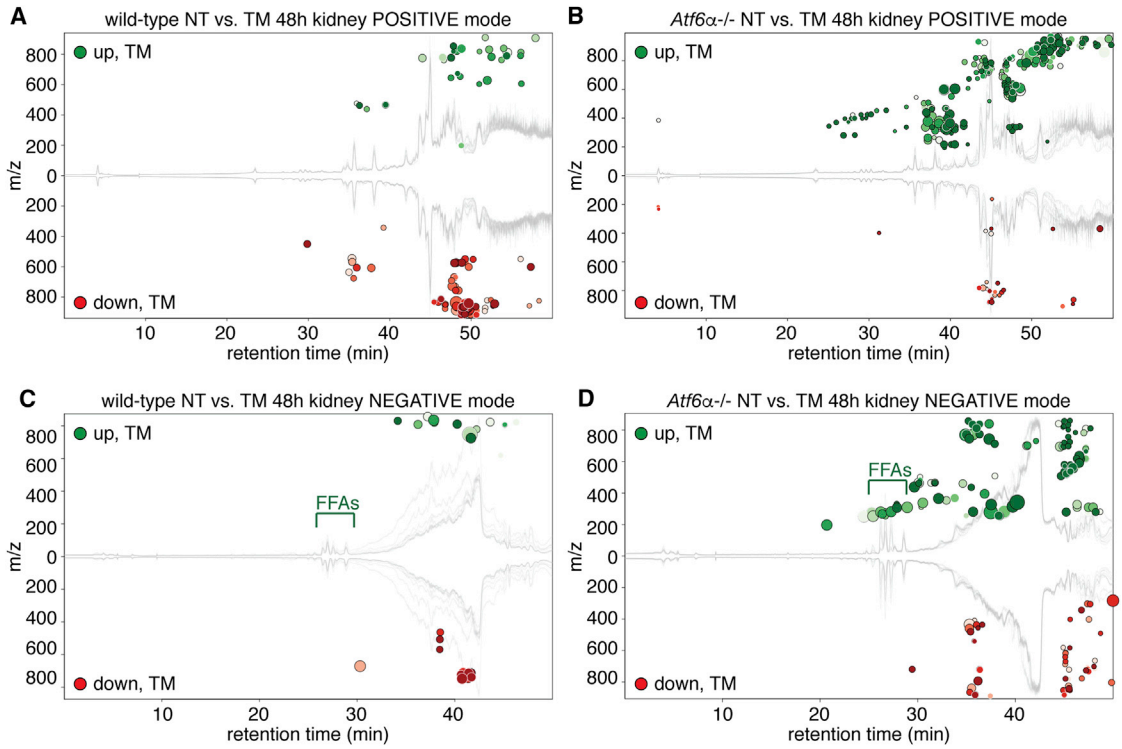

Figure 5. TM Treatment Leads to Quantifiable Lipid Accumulation in the Kidneys of Atf6$\alpha^{-/-}$ but Not Wild-Type Animals

(A–D) LC-MS in both positive and negative ion modes was used to profile the lipid distribution upon TM challenge in wild-type and *Atf6*$\alpha^{-/-}$ animals. (A) and (B) show positive mode, and (C) and (D) show negative mode. The response in wild-type animals is shown in (A) and (C), while the response in *Atf6*$\alpha^{-/-}$ animals is shown in (B) and (D). XCMS software was used to generate cloud plots to provide a global view of species that were significantly different between groups. The x axis shows retention time, and the y axis shows the mass-to-charge (m/z) ratio, with species upregulated by TM shown in green above the midline and downregulated species shown in red below the midline. The species shown are all those with a maximum intensity above 5,000 (i.e., to filter for reasonably abundant species) and an FDR-adjusted p value below 0.01. Darker circles have lower (i.e., more significant) p values, and the radius of each feature is proportional to the fold change. Position of FFAs is indicated. n = 4.

NT, not treated. See also Figure S1.

associated with elevated ceramides (Mather and Siskind, 2011; Ueda, 2015) (Figure S1). This finding suggests that ceramide synthesis is actively regulated by prolonged ER stress in the kidney—a finding that awaits mechanistic investigation.

Analysis in negative ion mode immediately suggested a potential pathway to lipid accumulation. Very few lipid species detected in this mode were changed by TM in wild-type animals (and of these, none could be putatively identified) (Figure 5C; Table 1). However, *Atf6*$\alpha^{-/-}$ animals evinced a substantial accumulation of free fatty acids (FFAs) (Figure 5D; Table 1). As FFAs are not the preferred form of cellular lipid storage and can, in fact, be lipotoxic (Neuschwander-Tetri, 2010), this finding suggested that the production (by lipogenesis or hepatic lipolysis) or import of FFAs outpaced the capacity of the kidneys to esterify them.

In order to confirm this accumulation of FFAs, the absolute concentrations of stearic, palmitic, oleic, and linoleic acids were quantified by comparison to standards. This analysis showed a significant accumulation of palmitic acid and even greater accumulations of oleic and linoleic acids (Figure 6A). The apparent preference for the accumulation of unsaturated fatty acids (FAs) might account for the similar accumulation of triglycerides with unsaturated FA chains (Table 1). These findings raised the possibility that the accumulation of FFAs might also contribute to liver steatosis in *Atf6*$\alpha^{-/-}$ animals. Indeed, 48 hr after TM treatment, there was a dramatic increase in FFAs in *Atf6*$\alpha^{-/-}$ animals, to the point that these were among the most abundant negative-mode lipids in the liver (Figure 6B). In contrast, there was no significant difference in FFAs in the livers of these animals 24 hr after treatment (data not shown), indicating that FFA accumulation is a late event.

The late accumulation of FFAs in both the liver and kidneys of *Atf6*$\alpha^{-/-}$ animals, as well as the absence of evidence for altered renal lipid anabolism or catabolism in these animals, led us to consider the possibility that this process is driven by lipolysis from adipose tissue. At early times after challenge, TM did not elicit a change in plasma levels of non-esterified fatty acids (NEFAs) (Figure 6C). In wild-type animals, this remained the case through later times (Figure 6D). However, *Atf6*$\alpha^{-/-}$ animals showed elevated plasma NEFA levels 48 hr after challenge, to an extent comparable to that elicited by prolonged fasting in wild-type animals (Figure 6D).

These results led us to suspect that unmitigated ER stress might suppress food consumption and drive fasting-induced lipolysis. Analysis of animals housed in metabolic cages

Table 1. Putative Lipid Identifications from LC-MS Analysis of the Kidney

Putative ID	Fold	p	Level	m/z	Retention Time (min)
Regulated by TM in the Kidney, Wild-Type Animals, POSITIVE Mode					
PC (38:3)	−2.3	0.0013	36,410	812.62	46.3
PE (P-40:5)	3.2*	0.0065	7,578	778.57	46.5
54:8 TG	−1.6	0.0084	25,736	892.75	51.7
48:3 TG	−1.6	0.0043	50,195	818.73	52.4
50:4 TG	−3.5	0.0000	71,882	844.74	52.9
PC (P-38:6)	2.0*	0.0034	5,092	790.57	56.1
TG (48:0)	−1.5	0.0068	20,852	824.78	58.3
Regulated by TM in the Kidney, *Atf6α*$^{-/-}$ Animals, POSITIVE Mode					
Linoleyl carnitine	2.1*	0.0002	13,944	424.34	29.0
Palmitoyl carnitine	1.6*	0.0013	16,189	400.34	29.7
Lyso-PAF C-16	3.0*	0.0065	6,483	482.36	36.8
PC (32:2)	4.5*	0.0027	38,593	730.54	44.3
PA (42:4)	2.8*	0.0020	20,999	781.56	44.3
PC (32:1)	2.1*	0.0046	154,864	732.56	45.0
PC (32:0)	2.1*	0.0051	18,978	734.56	45.0
PE (38:3)	2.2*	0.0024	7,374	770.58	45.1
PS (36:0)	−2.1	0.0058	22,716	809.59	45.5
PS (38:1)	−1.7	0.0093	15,486	835.61	46.0
PA (P-42:0)	1.7*	0.0067	14,692	773.65	46.8
CerP(d44:2)	2.3*	0.0070	5,808	801.68	46.9
GalCer(d40:2)	1.9*	0.0036	30,998	799.67	46.9
Behenyl linolenate	2.2*	0.0008	13,605	604.60	47.6
TG (52:6)	3.8*	0.0092	45,386	868.74	52.3
TG (54:8)	9.4*	0.0010	21,330	892.75	52.6
TG (58:9)	7.2*	0.0054	6,584	946.79	53.4
TG (58:8)	3.1*	0.0095	6,079	948.81	54.7
TG (54:6)	2.3*	0.0051	15,588	896.78	56.1
TG (56:6)	3.8*	0.0007	16,561	924.81	56.2
TG (56:7)	4.9*	0.0038	24,642	922.79	56.2
Regulated by TM in the Kidney, Wild-Type Animals, NEGATIVE Mode					
None identified					
Regulated by TM in the Kidney, *Atf6α*$^{-/-}$ Animals, NEGATIVE Mode					
C16:2 Fatty acid	11.7*	0.0081	6,994	251.20	24.5
C18:3 Fatty acid	7.7*	0.0081	9,365	277.22	25.3
C16:1 Fatty acid	9.9*	0.0073	23,028	253.22	25.4
C18:2 Fatty acid	8.7*	0.0042	159,391	279.23	26.2
C18:0 Fatty acid	2.1*	0.0058	6,731	283.24	26.6
C16:0 Fatty acid	2.2*	0.0059	159,497	255.23	26.7
C18:1 Fatty acid	7.9*	0.0024	140,480	281.25	27.3
C20:1 Fatty acid	9.8*	0.0041	8,325	309.28	28.9
Cer(d34:2)	3.2*	0.0003	31,934	534.49	45.0
Cer(d34:1)	2.5*	0.0002	50,804	536.50	45.6
Cer(d40:2)	2.5*	0.0053	21,262	618.58	47.2

Asterisks indicate upregulation by TM. m/z, mass-to-charge ratio; PE, phosphatidylethanolamine; PC, phosphatidylcholine, PA, phosphatidic acid; TG, triglyceride; PAF, platelet activating factor; PS, phosphatidylserine; GalCer, galactoyslceramide; CerP, ceramide phosphate; Cer, ceramide.

supported this hypothesis: TM treatment significantly reduced food intake in both wild-type and *Atf6α*$^{-/-}$ animals, and this reduction was exacerbated by 48 hr selectively in *Atf6α*$^{-/-}$ animals (Figure 6E). Consistent with this finding, by 48 hr, *Atf6α*$^{-/-}$ mice were severely hypoglycemic (Figure 6F). That this hypoglycemia was likely due to anorexia and not to hyperinsulinemia

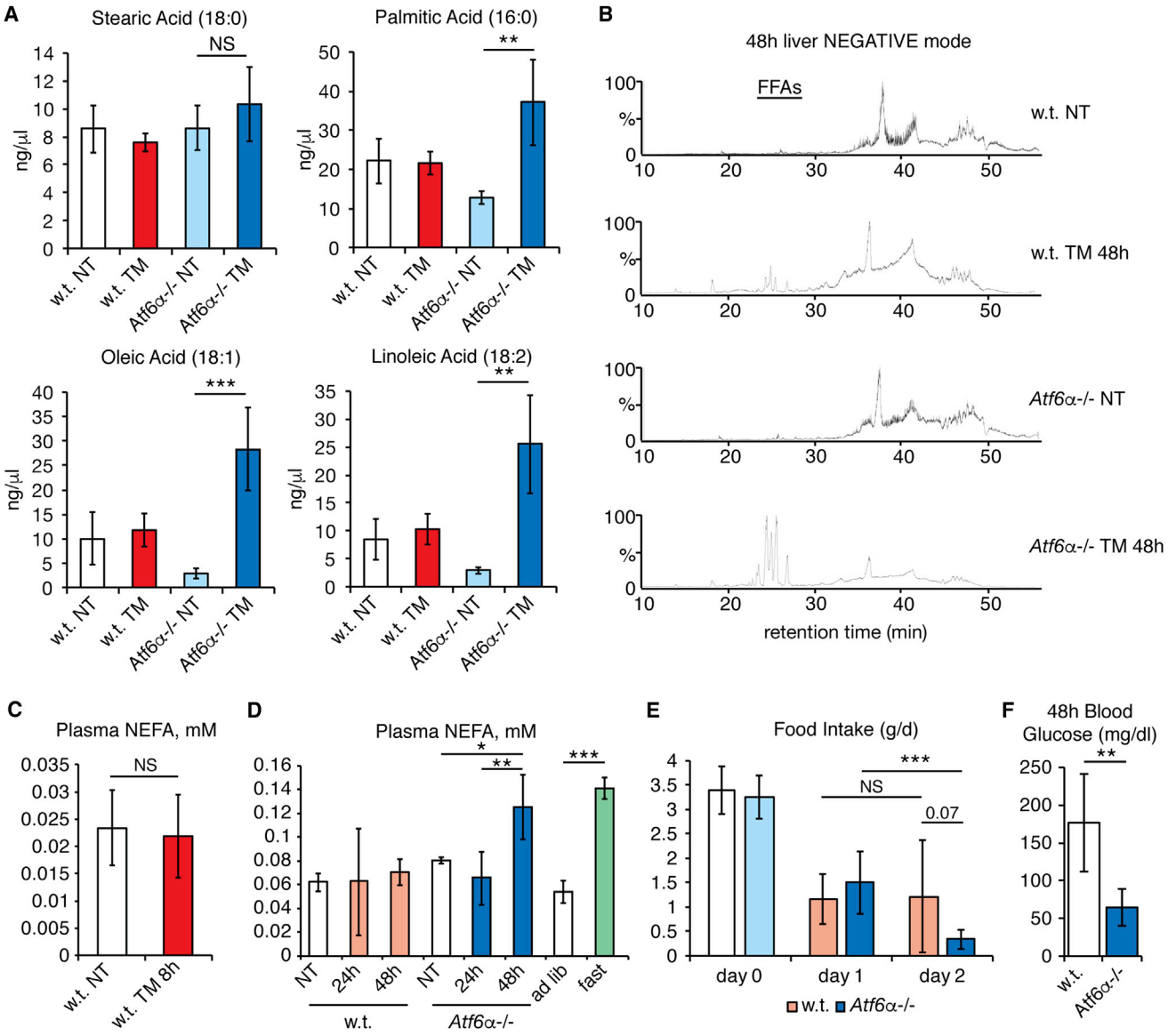

Figure 6. TM Treatment Increases Renal and Hepatic FFA Levels Preferentially in Atf6$\alpha^{-/-}$ Animals

(A) Renal levels of stearic, palmitic, oleic, and linoleic acids were quantified from LC runs of extracted lipids following 48 hr of TM treatment in wild-type (w.t.) or *Atf6*$\alpha^{-/-}$ animals. n = 4.

(B) Total ion chromatograms are shown from LC runs of hepatic lipids following 48 hr of TM treatment in wild-type or *Atf6*$\alpha^{-/-}$ animals. Retention time of FFAs is indicated. Each chromatogram shows a single representative animal.

(C) NEFAs were measured from plasma of wild-type animals fasted for 24 hr and treated for 8 hr with TM or vehicle. n = 8–9.

(D) NEFAs were measured from plasma of wild-type or *Atf6*$\alpha^{-/-}$ animals treated for 24 or 48 hr with TM. As a comparison, wild-type animals were also fed ad libitum or fasted for 24 hr. n = 3–6.

(E) Wild-type or *Atf6*$\alpha^{-/-}$ animals were habituated to metabolic cages, and food intake was measured either for the day preceding TM treatment (day 0) or for the periods 0–24 hr (day 1) or 24–48 hr (day 2) thereafter. Statistical significance comparing day 1 measurements to day 2 measurements was calculated using paired t tests, while significance comparing wild-type to *Atf6*$\alpha^{-/-}$ animals on day 2 used one-way ANOVA. n = 6–7.

(F) Plasma glucose levels were measured 48 hr after TM challenge in animals from (E).

*p < 0.05; **p < 0.01; ***p < 0.001; NS, not significant.

NT, not treated; CPM, counts per minute. See also Figure S2.

from stress-dependent pancreatic beta cell proliferation (Sharma et al., 2015) was supported by the observation that *Atf6*$\alpha^{-/-}$ mice did not become hyperinsulinemic during TM treatment (Figure S2B) but, if anything, tended toward hyperglycemia rather than hypoglycemia under unchallenged conditions (Figure S2C). It is also unlikely that lipolysis was driven by direct effects of TM on adipose, as we found no evidence that TM elicited ER stress in either subcutaneous or visceral white adipose deposits

(Figure S2D). These data point to anorexia-induced lipolysis as a potentially significant contributor to the late accumulation of FFAs in both the liver and kidneys of *Atf6α*$^{-/-}$ mice.

DISCUSSION

Our results suggest that ER stress has both cell-autonomous and cell-non-autonomous effects on peripheral lipid metabolism, with several pathways contributing to the accumulation of lipid in the liver and kidneys. In the liver, ER stress elicited the relatively rapid (within 8 hr) inhibition of FAox. While this inhibition was alleviated in wild-type animals, it persisted and was possibly exacerbated in *Atf6α*$^{-/-}$ animals. This persistence corresponded with the ongoing ER stress burden—owing to an inability to effectively harness the UPR to alleviate the stress (Wu et al., 2007; Yamamoto et al., 2007)—and with the profound suppression of FAox genes in these animals. Thus, we conclude that the inhibition of FAox likely contributes to stress-induced hepatic steatosis. This contribution would be in addition to the already described inhibition of VLDL secretion that would be expected to impair the efflux of triglyceride. This effect appears also to be liver specific, as we found no evidence for either genetic or biochemical inhibition of FAox in the kidney (Figure 4). We have previously shown that the inhibition of FAox protects ER function by enhancing the oxidative potential of the ER, which must generate disulfide bonds on nascent proteins (Tyra et al., 2012). It is tempting to speculate that the direct regulation of FAox represents an underappreciated mechanism by which the UPR protects ER homeostasis.

While lipogenesis has been proposed to contribute to ER stress-induced hepatic steatosis, based on studies in cultured hepatocytes (Lee et al., 2012), we found little evidence here that it is a significant contributor in vivo, at least at early times. There is, perhaps, an increase in lipogenic activity at later time points selectively in *Atf6α*$^{-/-}$ animals, although this observation is difficult to reconcile with the substantial suppression of both *Srebf* genes and of those encoding the key enzymes of lipogenesis. Thus, its potential role remains ambiguous. In the kidney, there was no evidence that lipogenesis contributed to fat accumulation, although we note that a previous report that suggested that ER stress causes renal lipid accumulation through an SREBP2-dependent mechanism (Lhoták et al., 2012). SREBP2 drives cholesterologenesis (Sato, 2010), and although *Hmgcr* (encoding the rate-limiting step in cholesterol biosynthesis) was not elevated by TM treatment, the lipogenesis assay used here does not extract cholesterol, making it still possible that SREBP2-dependent cholesterologenesis contributes to renal steatosis.

The other major contributor to both hepatic and renal steatosis appears to be anorexia-induced lipolysis. Indeed, the dramatic increase in both hepatic and renal FFAs at 48 hr was the most unexpected finding of the lipidomic analysis. The evidence that *Atf6α*$^{-/-}$ animals preferentially showed reduced food intake, hypoglycemia, and elevated plasma NEFA levels supports the idea that late lipid accumulation arises cell non-autonomously as a consequence of anorexia, particularly in the kidney. These elevated FFAs are presumably taken up by both organs, and some of it (though clearly not all) is esterified into triglyceride. However, we note that the rate of fatty acid uptake into the liver and kidney was not measured, since this measurement in vivo is complicated by both the instability and the rapid oxidation of labeled FFA probes (Henkin et al., 2012). A survey of the expression of fatty acid transport genes in liver and kidney revealed some that were suppressed by stress and others that were unaffected (data not shown), technically leaving open the question of whether the elevated levels of FFAs seen here, in fact, lead to increased renal and hepatic FFA levels. In any case, it will be interesting to determine whether the observed starvation and resultant lipolysis occurs merely as a result of *Atf6α*$^{-/-}$ animals experiencing severe illness due to kidney and/or liver dysfunction or whether, instead, there are effects of TM administration on tissues other than the liver and kidney in these animals that drive lipolysis. For instance, it is also possible that lipolysis is driven by the effects of ATF6α deletion in white adipose, although the fact that we did not find evidence of TM-induced ER stress in the adipose (Figure S2D) makes this possibility somewhat unlikely.

Ultimately, the reason that *Atf6α*$^{-/-}$ animals eventually succumb to TM challenge (Wu et al., 2007), while wild-type animals do not, remains unclear. Given that *Atf6α*$^{-/-}$ animals show evidence of cell death in the kidney (Figure S1B), one possibility is that unmitigated ER stress in the *Atf6α*$^{-/-}$ kidney damages the organ beyond repair through extensive apoptosis and/or necrosis. Indeed, one of the other notable features of our lipidomic analysis was the elevation of several species putatively identified as ceramides (Table 1), which are known mediators of cell-death pathways and serve as biomarkers for renal injury (Mather and Siskind, 2011; Ueda, 2015). We also favor the kidney as the most probable primary site of TM-induced anorexia in *Atf6α*$^{-/-}$ mice, in part because the liver—the other organ most clearly targeted by TM—while clearly adversely affected by ER stress in these animals, is so resilient to lipid accumulation and cell loss (Forbes and Newsome, 2016). In sum, the data here are most consistent with a model in which ER stress in the liver directly regulates lipid metabolism in the organ, while unmitigated ER stress in the kidney and/or liver drives lipolysis from the white adipose to further dysregulate metabolism in these organs. If this is the case, then it is possible that physiological ER stress localized in a given tissue can, nonetheless, drive lipid dysregulation in other sites not directly experiencing ER stress. Ultimately, the tissue-specific deletion of ATF6α will be needed to address the relative contributions of liver, kidney, and other organs to the extreme sensitivity of *Atf6α*$^{-/-}$ animals to TM and to determine how the ER stress signaling network interacts with other regulators of metabolism, such as CREBH (Zhang et al., 2012) and CRTC2 (Wang et al., 2009).

Although other stressors, such as proteasome inhibition or secretory protein overexpression, also lead to hepatic steatosis and similar changes in gene regulation, at least in the liver—making it unlikely that the effects seen here are specific to TM per se—the agent is, nonetheless, probably a much harsher stimulus than those that lead to lipid dysregulation in vivo. Thus, moving forward, it will be important to determine the extent to which more physiological ER stresses impinge upon lipid metabolism in the ways described here.

EXPERIMENTAL PROCEDURES

Mice

Animals were housed in a pathogen-free facility under climate controlled conditions with a 12 hr light/dark cycle, and were maintained on standard rodent chow. All procedures were approved by the University of Iowa Institutional Animal Care and Use Committee. *Atf6α*$^{-/-}$ animals have been backcrossed into the *C57BL/6J* strain for more than ten generations. Eight-to-10 week-old animals of both genders were injected intraperitoneally with either 1 mg/kg TM (EMD) dissolved in DMSO and diluted in 150 mM dextrose or PBS or an equivalent concentration of DMSO alone in dextrose or PBS (for all non-treated animals). At sacrifice, plasma was collected, and liver and kidney tissues were harvested and were either used fresh (for biochemical assays), fixed in formalin (for immunostaining), frozen in OCT (for oil red O staining), or flash frozen in liquid N_2 (for molecular analysis and MS). Tissue triglyceride measurement (Arensdorf et al., 2013a), immunostaining (Chikka et al., 2013), oil red O staining (Arensdorf et al., 2013a), and qRT-PCR (Rutkowski et al., 2006) were performed as described. For metabolic cage experiments, animals were habituated to cages for 5 days and then treated with 1 mg/kg TM and monitored for a further 2 days.

Lipogenesis Assay

Lipogenesis assays were performed on fresh tissue homogenates, modifying a protocol described by Harada et al. (2007). Briefly, liver was placed on ice, and 60 mg was macerated into small pieces and added to 2 mL DMEM, which had been aerated in 5% CO_2/95% O_2 for 20 min. 6 μCi of [1-^{14}C] sodium acetate was added, and samples were incubated for 90 min at 37°C in 5% CO_2/95% O_2. The tissue was removed, dabbed with an absorbent wipe, and added to 300 μL of 30% w/v KOH heated to 70°C, with agitation for 10 min; then 300 μL 100% ethanol was added prior to continued incubation at 70°C, with agitation for 2 hr. At this point, protein concentration was measured from an aliquot, while the remainder of the sample was chilled on ice and then acidified with 300 μLof 9 M H_2SO_4. Lipids were extracted three times with 500 μL light petroleum (boiling point [bp], 40°C–60°C). The petroleum fractions were combined and washed three times with deionized water. They were then evaporated to dryness under nitrogen gas and then dissolved in scintillation fluid for ^{14}C quantification. For 8-hr TM treatment, animals were also treated with 2 U human insulin intraperitoneally to ensure that conditions favored lipogenesis activity.

FAox Assays

FAox assays were performed on fresh tissue generally, as described previously (Hirschey and Verdin, 2010), in animals fasted for 24 hr to ensure that conditions favored FAox activity. Briefly, 150 mg tissue was added to 1 mL ice-cold STE Buffer (0.25 M sucrose, 10 mM Tris (pH 7.4), 1 mM EDTA), and the tissue was homogenized in a dounce homogenizer. The homogenate was centrifuged at 4°C for 10 min at 420 × *g*. A portion of the supernatant was reserved to determine protein concentration. 20 μL of the supernatant was added to 355 μL reaction mixture (100 mM sucrose, 10 mM Tris (pH 7.4), 5 mM KH_2PO_4, 0.2 mM EDTA, 0.3% FFA-free BSA, 80 mM KCl, 2 mM L-carnitine, 0.1 mM malic acid, 0.05 mM CoA, 1 mM $MgCl_2$, with 1 mM DTT and 2 mM ATP added fresh). Then 25 μL of a mixture containing 0.1 mM palmitic acid, 7.5% fatty-acid-free BSA, and 4 μCi of [1-^{14}C] palmitic acid was added, and the reaction was incubated with agitation at 37°C for 60 min. Following incubation, the samples were transferred to new tubes containing 200 μL of 1 M perchloric acid fitted in the lid with Whatmann 3-mm filter paper soaked in 1 M NaOH. Samples were capped immediately and incubated at room temperature for 1 hr, and then the filter paper discs were removed and transferred to scintillation fluid for ^{14}C quantification. Etomoxir was from Sigma. To measure plasma β-hydroxybutyrate, the Ketone Body Assay Kit (Cayman Chemical) was used.

For FAox in isolated mitochondria, mitochondria were isolated from ~150 mg of fresh liver tissue using differential centrifugation as previously described (Gray et al., 2016).^{14}C-palmitate oxidation was measured as previously described (Sheldon et al., 2015). In brief, mitochondria were placed in an air-tight well with reaction media containing 20 μM palmitate conjugated to BSA. After 1 hr, 70% perchloric acid was injected into the well to liberate $^{14}CO_2$, which was trapped in a microcentrifuge tube containing 1 N NaOH. $^{14}CO_2$ containing NaOH and ^{14}C acid-soluble metabolites (ASMs) were quantified via liquid scintillation counting. Media-specific activity and blank samples (no mitochondria) were used to convert raw dpm counts to micromole per gram of protein per hour.

MS

For MS analysis, frozen tissue pieces were pulverized using a metal cup and mallet. 100 mg frozen tissue powder was added to 2 mL of a 2:1 chloroform:methanol mixture in a 5-mL glass flat-bottom tube with a Teflon cap liner. Heptadecanoic acid was spiked into the sample at 0.5 ng/μL as an internal standard. The sample was sonicated on ice with a probe sonicator for 60 s; then 1 mL of H_2O was added, and the sample was vortexed for 30 s, incubated on ice for 30 min, and revortexed. Following centrifugation for 15 min at 200 × *g* at 4°C, the bottom layer was removed, transferred to a new tube, dried under a stream of nitrogen gas, and resuspended in 200 μL of 2:1 chloroform:methanol.

The samples were analyzed by LC-MS using a Waters Q-TOF (quadrupole time-of-flight) Premier mass spectrometer interfaced with an Acquity UPLC (ultra-performance liquid chromatography) system. ESI was used, and data were collected in both positive and negative ion modes using leucine enkephalin as the lock mass. The MS conditions were as follows for both positive and negative ESI: capillary voltage, 2.8 kV; sampling cone voltage, 35 V; source temperature, 110°C; desolvation gas temperature, 400°C; cone gas flow, 30 L/hr; and desolvation gas flow, 750 L/hr. Data were collected over the mass range, 130 to 1,000 Da.

The chromatographic separation was performed using a Phenomenex Gemini C18 column (4.6 mm × 50 mm, 5 μm). The mobile phase was 95:5 water/methanol (v/v) in solvent A and 65:35:5 isopropanol/methanol/water (v/v/v) in solvent B. Depending on whether positive or negative ESI was being used, either 0.1% formic acid or ammonium hydroxide was added to both solvents, respectively. The gradient initially held for 5 min at 100% solvent A at a flow rate of 100 μL/min. At 5.1 min, flow rate increased to 400 μL/min. Over the next 40 min, gradient increased to 100% solvent B, at which point, the flow rate was increased to 500 μL/min. The system was held at 100% solvent B for 18 min and then re-equilibrated back to 100% solvent A over 7 min. Injection volume was 15 μL for all samples. The column was held at 25°C throughout the run.

LC-MS data acquisition and analysis were performed by using Waters MassLynx software. The quantification of the fatty acids was performed utilizing QuanLynx software package using standard curves for oleic, linoleic, palmitic, and stearic acids. Otherwise, the data files were converted to NetCDF format using DataBridge conversion software for further processing in XCMS. CDF files were uploaded to the XCMS website (http://xcmsonline.scripps.edu) to create individual datasets. The datasets were then compared using pairwise analysis with the UPLC/Q-TOF parameter. The results table was filtered using the following parameters: FDR (false discovery rate)-adjusted p value $\leq$ 0.01, fold $\geq$ 1.5, and maximum intensity $\geq$ 5,000. These same parameters were applied to generate the red/green cloud plots. The mass-to-charge ratio from the species that fit the parameters was entered into the Lipid Maps online website search tool for the LIPID MAPS Structure Database (http://www.lipidmaps.org/data/structure/) and Metlin, with the following parameters: [M+NH4]+ and [M+H]+ (for positive run), [M−H]− (for negative run), mass tolerance of 0.1. The top hit was chosen for the lipid ID, after adjustment for the most plausible adducts, given the LC conditions. For triglycerides, the top hit that had all even chain carbons was chosen for the ID. Data are deposited in the Metabolights database (http://www.ebi.ac.uk/metabolights/).

Statistics

Throughout the paper, error bars represent means ± SD. Unless indicated otherwise, significance was calculated by one-way ANOVA with Tukey's post hoc where appropriate. Symbols to denote significance are as follows: *p < 0.05; **p < 0.01; ***p < 0.001. For all animal experiments, n represents the number of individual animals per group.

SUPPLEMENTAL INFORMATION

Supplemental Information includes two figures and can be found with this article online at http://dx.doi.org/10.1016/j.celrep.2017.05.020.

AUTHOR CONTRIBUTIONS

All authors read, edited, and approved the manuscript. D.D.-M. and D.T.R. conceived and designed the experiments, analyzed the data, and wrote the paper. D.D.-M. performed most of the experiments prior to review, and E.R.G. performed or assisted on experiments for revision. R.D.S. performed mitochdondria FAox experiments. D.-F.G. performed metabolic cage experiments. R.J.K. provided *Atf6*$\alpha^{-/-}$ mice. E.B.T., K.R., M.P.G., and L.M.T contributed to data analysis. M.C.G., M.P.G., and L.M.T. contributed to MS experiments and data analysis.

ACKNOWLEDGMENTS

We thank A. Norris (University of Iowa Department of Pediatrics) for assistance with FAox assays and R. McCabe for assistance with MS data processing. Funding sources were as follows: NIH grant GM115424 and funds from the University of Iowa Department of Anatomy and Cell Biology, the Carver College of Medicine, and the Office of the Vice President for Research (OVPR) (to D.T.R.); American Heart Association (AHA) training grant 14POST20420015 (to D.D.-M.); NIH training grant HL07734 (to R.D.S.); NIH grant DK104998 and a University of Iowa Healthcare Research Investment Pilot Grant (to E.B.T.); funds from the OVPR (to L.M.T.); NIH grant HL084207, AHA grant 14EIA18860041, and funds from the University of Iowa Fraternal Order of Eagles Diabetes Research Center (to K.R.); NIH grants DK042394, DK103185, DK110973, and CA198103 (to R.J.K.); and the Novo Nordisk Foundation Center for Basic Metabolic Research, an independent research center at the University of Copenhagen, partially funded by an unrestricted donation from the Novo Nordisk Foundation (http://www.metabol.ku.dk) (to M.P.G.).

Received: October 24, 2016
Revised: March 31, 2017
Accepted: May 4, 2017
Published: May 30, 2017

REFERENCES

Adachi, Y., Yamamoto, K., Okada, T., Yoshida, H., Harada, A., and Mori, K. (2008). ATF6 is a transcription factor specializing in the regulation of quality control proteins in the endoplasmic reticulum. Cell Struct. Funct. *33*, 75–89.

Arensdorf, A.M., Dezwaan McCabe, D., Kaufman, R.J., and Rutkowski, D.T. (2013a). Temporal clustering of gene expression links the metabolic transcription factor HNF4α to the ER stress-dependent gene regulatory network. Front. Genet. *4*, 188.

Arensdorf, A.M., Diedrichs, D., and Rutkowski, D.T. (2013b). Regulation of the transcriptome by ER stress: non-canonical mechanisms and physiological consequences. Front. Genet. *4*, 256.

Azuma, Y., Hagiwara, D., Lu, W., Morishita, Y., Suga, H., Goto, M., Banno, R., Sugimura, Y., Oyadomari, S., Mori, K., et al. (2014). Activating transcription factor 6α is required for the vasopressin neuron system to maintain water balance under dehydration in male mice. Endocrinology *155*, 4905–4914.

Cao, S.S., Zimmermann, E.M., Chuang, B.M., Song, B., Nwokoye, A., Wilkinson, J.E., Eaton, K.A., and Kaufman, R.J. (2013). The unfolded protein response and chemical chaperones reduce protein misfolding and colitis in mice. Gastroenterology *144*, 989–1000.e6.

Chan, S.W. (2014). Unfolded protein response in hepatitis C virus infection. Front. Microbiol. *5*, 233.

Chikka, M.R., McCabe, D.D., Tyra, H.M., and Rutkowski, D.T. (2013). C/EBP homologous protein (CHOP) contributes to suppression of metabolic genes during endoplasmic reticulum stress in the liver. J. Biol. Chem. *288*, 4405–4415.

Colgan, S.M., Tang, D., Werstuck, G.H., and Austin, R.C. (2007). Endoplasmic reticulum stress causes the activation of sterol regulatory element binding protein-2. Int. J. Biochem. Cell Biol. *39*, 1843–1851.

Egawa, N., Yamamoto, K., Inoue, H., Hikawa, R., Nishi, K., Mori, K., and Takahashi, R. (2011). The endoplasmic reticulum stress sensor, ATF6α, protects against neurotoxin-induced dopaminergic neuronal death. J. Biol. Chem. *286*, 7947–7957.

Forbes, S.J., and Newsome, P.N. (2016). Liver regeneration - mechanisms and models to clinical application. Nat. Rev. Gastroenterol. Hepatol. *13*, 473–485.

Gibbons, G.F., Wiggins, D., Brown, A.M., and Hebbachi, A.M. (2004). Synthesis and function of hepatic very-low-density lipoprotein. Biochem. Soc. Trans. *32*, 59–64.

Gomez, J.A., Tyra, H.M., DeZwaan-McCabe, D., Olivier, A.K., and Rutkowski, D.T. (2014). Synthetic embryonic lethality upon deletion of the ER cochaperone p58(IPK) and the ER stress sensor ATF6α. Biochem. Biophys. Res. Commun. *443*, 115–119.

Gray, L.R., Rauckhorst, A.J., and Taylor, E.B. (2016). A method for multiplexed measurement of mitochondrial pyruvate carrier activity. J. Biol. Chem. *291*, 7409–7417.

Harada, N., Oda, Z., Hara, Y., Fujinami, K., Okawa, M., Ohbuchi, K., Yonemoto, M., Ikeda, Y., Ohwaki, K., Aragane, K., et al. (2007). Hepatic de novo lipogenesis is present in liver-specific ACC1-deficient mice. Mol. Cell. Biol. *27*, 1881–1888.

Harding, H.P., Zeng, H., Zhang, Y., Jungries, R., Chung, P., Plesken, H., Sabatini, D.D., and Ron, D. (2001). Diabetes mellitus and exocrine pancreatic dysfunction in perk-/- mice reveals a role for translational control in secretory cell survival. Mol. Cell *7*, 1153–1163.

Henkin, A.H., Cohen, A.S., Dubikovskaya, E.A., Park, H.M., Nikitin, G.F., Auzias, M.G., Kazantzis, M., Bertozzi, C.R., and Stahl, A. (2012). Real-time noninvasive imaging of fatty acid uptake in vivo. ACS Chem. Biol. *7*, 1884–1891.

Herrema, H., Zhou, Y., Zhang, D., Lee, J., Salazar Hernandez, M.A., Shulman, G.I., and Ozcan, U. (2016). XBP1s is an anti-lipogenic protein. J. Biol. Chem. *291*, 17394–17404.

Hirschey, M.D., and Verdin, E. (2010). Measuring fatty acid oxidation in tissue homogenates. Protoc. Exch. Published online April 15, 2010. http://dx.doi.org/10.1038/nprot.2010.92.

Hirschey, M.D., Shimazu, T., Jing, E., Grueter, C.A., Collins, A.M., Aouizerat, B., Stančáková, A., Goetzman, E., Lam, M.M., Schwer, B., et al. (2011). SIRT3 deficiency and mitochondrial protein hyperacetylation accelerate the development of the metabolic syndrome. Mol. Cell *44*, 177–190.

Ji, C. (2014). New insights into the pathogenesis of alcohol-induced ER stress and liver diseases. Int. J. Hepatol. *2014*, 513787.

Jones, J.G. (2016). Hepatic glucose and lipid metabolism. Diabetologia *59*, 1098–1103.

Lee, J.S., Mendez, R., Heng, H.H., Yang, Z.Q., and Zhang, K. (2012). Pharmacological ER stress promotes hepatic lipogenesis and lipid droplet formation. Am. J. Transl. Res. *4*, 102–113.

Lhoták, S., Sood, S., Brimble, E., Carlisle, R.E., Colgan, S.M., Mazzetti, A., Dickhout, J.G., Ingram, A.J., and Austin, R.C. (2012). ER stress contributes to renal proximal tubule injury by increasing SREBP-2-mediated lipid accumulation and apoptotic cell death. Am. J. Physiol. Renal Physiol. *303*, F266–F278.

Mather, A.R., and Siskind, L.J. (2011). Glycosphingolipids and kidney disease. Adv. Exp. Med. Biol. *721*, 121–138.

Neuschwander-Tetri, B.A. (2010). Nontriglyceride hepatic lipotoxicity: the new paradigm for the pathogenesis of NASH. Curr. Gastroenterol. Rep. *12*, 49–56.

Ota, T., Gayet, C., and Ginsberg, H.N. (2008). Inhibition of apolipoprotein B100 secretion by lipid-induced hepatic endoplasmic reticulum stress in rodents. J. Clin. Invest. *118*, 316–332.

Özcan, U., Cao, Q., Yilmaz, E., Lee, A.H., Iwakoshi, N.N., Ozdelen, E., Tuncman, G., Görgün, C., Glimcher, L.H., and Hotamisligil, G.S. (2004). Endoplasmic reticulum stress links obesity, insulin action, and type 2 diabetes. Science *306*, 457–461.

Rui, L. (2014). Energy metabolism in the liver. Compr. Physiol. *4*, 177–197.

Rutkowski, D.T., Arnold, S.M., Miller, C.N., Wu, J., Li, J., Gunnison, K.M., Mori, K., Sadighi Akha, A.A., Raden, D., and Kaufman, R.J. (2006). Adaptation to ER stress is mediated by differential stabilities of pro-survival and pro-apoptotic mRNAs and proteins. PLoS Biol. *4*, e374.

Rutkowski, D.T., Wu, J., Back, S.H., Callaghan, M.U., Ferris, S.P., Iqbal, J., Clark, R., Miao, H., Hassler, J.R., Fornek, J., et al. (2008). UPR pathways combine to prevent hepatic steatosis caused by ER stress-mediated suppression of transcriptional master regulators. Dev. Cell *15*, 829–840.

Sato, R. (2010). Sterol metabolism and SREBP activation. Arch. Biochem. Biophys. *501*, 177–181.

Sharma, R.B., O'Donnell, A.C., Stamateris, R.E., Ha, B., McCloskey, K.M., Reynolds, P.R., Arvan, P., and Alonso, L.C. (2015). Insulin demand regulates β cell number via the unfolded protein response. J. Clin. Invest. *125*, 3831–3846.

Sheldon, R.D., Padilla, J., Jenkins, N.T., Laughlin, M.H., and Rector, R.S. (2015). Chronic NOS inhibition accelerates NAFLD progression in an obese rat model. Am. J. Physiol. Gastrointest. Liver Physiol. *308*, G540–G549.

Targett-Adams, P., McElwee, M.J., Ehrenborg, E., Gustafsson, M.C., Palmer, C.N., and McLauchlan, J. (2005). A PPAR response element regulates transcription of the gene for human adipose differentiation-related protein. Biochim. Biophys. Acta *1728*, 95–104.

Tyra, H.M., Spitz, D.R., and Rutkowski, D.T. (2012). Inhibition of fatty acid oxidation enhances oxidative protein folding and protects hepatocytes from endoplasmic reticulum stress. Mol. Biol. Cell *23*, 811–819.

Ueda, N. (2015). Ceramide-induced apoptosis in renal tubular cells: a role of mitochondria and sphingosine-1-phoshate. Int. J. Mol. Sci. *16*, 5076–5124.

Usui, M., Yamaguchi, S., Tanji, Y., Tominaga, R., Ishigaki, Y., Fukumoto, M., Katagiri, H., Mori, K., Oka, Y., and Ishihara, H. (2012). Atf6α-null mice are glucose intolerant due to pancreatic β-cell failure on a high-fat diet but partially resistant to diet-induced insulin resistance. Metabolism *61*, 1118–1128.

Walter, P., and Ron, D. (2011). The unfolded protein response: from stress pathway to homeostatic regulation. Science *334*, 1081–1086.

Wang, M., and Kaufman, R.J. (2016). Protein misfolding in the endoplasmic reticulum as a conduit to human disease. Nature *529*, 326–335.

Wang, Y., Vera, L., Fischer, W.H., and Montminy, M. (2009). The CREB coactivator CRTC2 links hepatic ER stress and fasting gluconeogenesis. Nature *460*, 534–537.

Wang, S., Chen, Z., Lam, V., Han, J., Hassler, J., Finck, B.N., Davidson, N.O., and Kaufman, R.J. (2012). IRE1α-XBP1s induces PDI expression to increase MTP activity for hepatic VLDL assembly and lipid homeostasis. Cell Metab. *16*, 473–486.

Wu, J., Rutkowski, D.T., Dubois, M., Swathirajan, J., Saunders, T., Wang, J., Song, B., Yau, G.D., and Kaufman, R.J. (2007). ATF6alpha optimizes long-term endoplasmic reticulum function to protect cells from chronic stress. Dev. Cell *13*, 351–364.

Wu, J., Ruas, J.L., Estall, J.L., Rasbach, K.A., Choi, J.H., Ye, L., Boström, P., Tyra, H.M., Crawford, R.W., Campbell, K.P., et al. (2011). The unfolded protein response mediates adaptation to exercise in skeletal muscle through a PGC-1α/ATF6α complex. Cell Metab. *13*, 160–169.

Yamamoto, K., Sato, T., Matsui, T., Sato, M., Okada, T., Yoshida, H., Harada, A., and Mori, K. (2007). Transcriptional induction of mammalian ER quality control proteins is mediated by single or combined action of ATF6alpha and XBP1. Dev. Cell *13*, 365–376.

Yamamoto, K., Takahara, K., Oyadomari, S., Okada, T., Sato, T., Harada, A., and Mori, K. (2010). Induction of liver steatosis and lipid droplet formation in ATF6alpha-knockout mice burdened with pharmacological endoplasmic reticulum stress. Mol. Biol. Cell *21*, 2975–2986.

Yoshikawa, A., Kamide, T., Hashida, K., Ta, H.M., Inahata, Y., Takarada-Iemata, M., Hattori, T., Mori, K., Takahashi, R., Matsuyama, T., et al. (2015). Deletion of Atf6α impairs astroglial activation and enhances neuronal death following brain ischemia in mice. J. Neurochem. *132*, 342–353.

Zhang, K., Wang, S., Malhotra, J., Hassler, J.R., Back, S.H., Wang, G., Chang, L., Xu, W., Miao, H., Leonardi, R., et al. (2011). The unfolded protein response transducer IRE1α prevents ER stress-induced hepatic steatosis. EMBO J. *30*, 1357–1375.

Zhang, C., Wang, G., Zheng, Z., Maddipati, K.R., Zhang, X., Dyson, G., Williams, P., Duncan, S.A., Kaufman, R.J., and Zhang, K. (2012). Endoplasmic reticulum-tethered transcription factor cAMP responsive element-binding protein, hepatocyte specific, regulates hepatic lipogenesis, fatty acid oxidation, and lipolysis upon metabolic stress in mice. Hepatology *55*, 1070–1082.